Current Biology 18, 81–90, January 22, 2008 ©2008 Elsevier Ltd All rights reserved DOI 10.1016/j.cub.2007.12.019

Article

Pericentric Chromatin Is Organized into an Intramolecular Loop in Mitosis

Elaine Yeh,[1,2] Julian Haase,[1,2] Leocadia V. Paliulis,[1] Ajit Joglekar,[1] Lisa Bond,[1] David Bouck,[1] E.D. Salmon,[1] and Kerry S. Bloom[1,*]
[1]Department of Biology
623 Fordham Hall CB#3280
University of North Carolina at Chapel Hill
Chapel Hill, North Carolina 27599-3280

Summary

Background: Cohesin proteins link sister chromatids and provide the basis for tension between bioriented sister chomatids in mitosis. Cohesin is concentrated at the centromere region of the chromosome despite the fact that sister centromeres can be separated by 800 nm in vivo. The function of cohesin at sites of separated DNA is unknown.
Results: We provide evidence that the kinetochore promotes the organization of pericentric chromatin into a cruciform in mitosis such that centromere-flanking DNA adopts an intramolecular loop, whereas sister-chromatid arms are paired intermolecularly. Visualization of cohesin subunits by fluorescence microscopy revealed a cylindrical structure that encircles the central spindle and spans the distance between sister kinetochores. Kinetochore assembly at the apex of the loop initiates intrastrand loop formation that extends approximately 25 kb (12.5 kb on either side of the centromere). Two centromere loops (one from each sister chromatid) are stretched between the ends of sister-kinetochore microtubules along the spindle axis. At the base of the loop there is a transition to intermolecular sister-chromatid pairing.
Conclusions: The C loop conformation reveals the structural basis for sister-kinetochore clustering in budding yeast and for kinetochore biorientation and thus resolves the paradox of maximal interstrand separation in regions of highest cohesin concentration.

Introduction

During mitosis, the eukaryotic cell constructs a bipolar array of microtubules (MTs) that serves as the machinery to segregate duplicated chromosomes. The centromere on each sister chromatid specifies the assembly of the kinetochore, a DNA-protein complex that interacts with the plus ends of kinetochore MTs (kMTs). Sister kinetochores can attach to MTs emanating from either pole, leading to configurations in which sister kinetochores are attached to opposite poles (amphitelic), sister kinetochores are attached to same poles (syntelic), or one kinetochore is attached to both poles (merotelic). The correct MT arrangement that persists is the one in which sister kinetochores are attached to opposite poles. Tension produced by amphitelic attachment is the probable basis for the stability of this configuration. The budding yeast *S. cerevisiae* has only one MT attachment per kinetochore and is an ideal system to characterize the force-producing mechanisms and tension elements that reside at the interface of kinetochore-MT attachments.

The physical linkage of sister chromatids is the mechanism for generation of tension for amphitelic attachment. This linkage is mediated by a multisubunit complex, cohesin, composed of two members of the structural maintenance of chromosomes (SMC) family of ATPases, Smc1 and Smc3, and two non-SMC subunits, Mcd1/Scc1 and Scc3 [1, 2]. Cohesin is associated with chromosomes from G_1 in the cell cycle until the onset of anaphase. It has been assumed that cohesin promotes association between sister chromatids (intermolecular linkage), and that is the basis for tension when sister chromatids are oriented to opposite spindle-pole bodies (SPBs). The Scc1 subunit disappears from chromosomes when sisters separate at the metaphase/anaphase transition. Scc1 is cleaved by separase upon anaphase onset. The discovery of cohesin dispelled the view that sister chromatids might be held via intercatenation of sister DNAs that was resolved at anaphase due to microtubule-pulling forces.

Cohesins can form ring-shaped structures in vitro, leading to several hypotheses that describe how these proteins connect sister chromatids [1, 2]. These include the embrace model, in which the complex forms a ring around sister DNA helices; the snap model, in which each cohesin complex binds a single DNA helix and linkage occurs through the association of two complexes; and the bracelet model, in which cohesin complexes oligomerize to wrap around sister DNA helices.

Genome-wide chromatin immunoprecipitation (ChIP) in budding yeast has revealed the predominant sites of cohesin binding [3, 4]. Most notable is the finding that cohesin is enriched ~3-fold in a 20–50 kb domain flanking the centromere, relative to the concentration of cohesin on chromosome arms. Although the location of cohesin along the length of the yeast chromosome has been established, little is known about how the concentration of cohesin within pericentric chromatin contributes to the fidelity of chromosome segregation.

The ability to visualize budding-yeast chromosomes in live cells revealed that sister kinetochores are separated before anaphase, as occurs in mammalian cells. Repeated arrays of the lac operator (*E. coli* lacO) were inserted into the yeast genome. Introduction of lac repressor-GFP allowed visualization of specific chromosomal domains [5]. Placement of the lacO array at varying distances from the centromere revealed that chromosome arms were closely apposed, whereas pericentric chromatin is stretched poleward in mitosis, prior to anaphase onset (Figure 1) [6–9]. Sister centromeres on a single chromosome oscillate relative to each other and often are separated by distances of up to 800 nm. The oscillation in separation distance suggests that the pericentromere regions of the chromosome are elastic, stretching in response to their dynamic kMT attachments. With GFP-fusion proteins used to mark centromeres of all chromosomes (centromeric histone H3 variant Cse4 [9, 10], and the inner kinetochore component Mtw1 [6]), it was found that sister kinetochores are organized into two lobes on either side of the equator of the metaphase spindle. This bipolar alignment is indicative of sister-centromere separation prior to anaphase. Subsequent visualization of a number

*Correspondence: kbloom@email.unc.edu
[2]These authors contributed equally to this work.

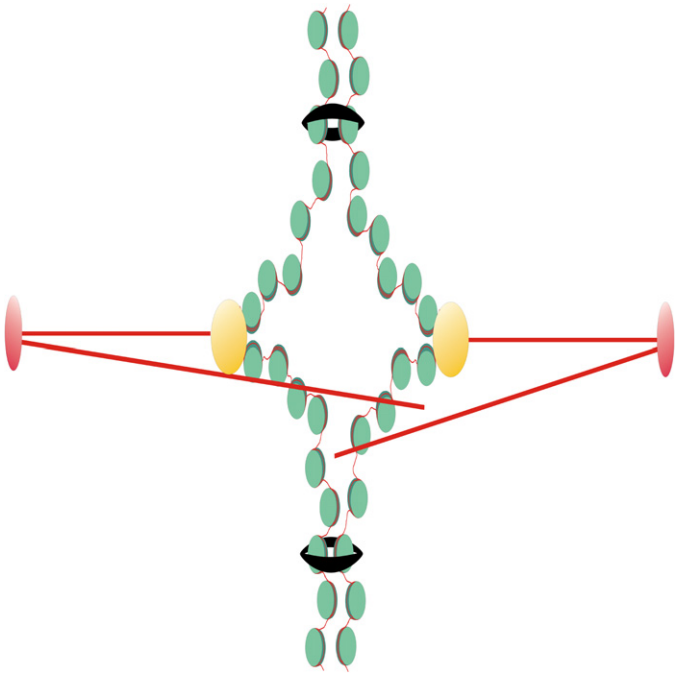

Figure 1. Organization of a Mitotic Chromosome

Chromosome arms are closely apposed and held together via cohesin (black rings). Sister kinetochores (yellow) are attached to kinetochore microtubules (red), and the pericentric chromatin is stretched toward the spindle poles. There are 16 chromosomes in yeast and 16 kinetochore microtubules in each spindle half. Cohesion between sister chromatids provides a mechanism to resist microtubule-pulling forces and generate tension at centromeres. The function of cohesin in pericentric chromatin is not well understood.

of kinetochore proteins and examination of their behavior after photobleaching [11] have substantiated the finding that sister centromeres are pulled apart by sister-kinetochore pulling forces in metaphase. The major paradox in the field is the accumulation and function of cohesin at sites of sister-chromatid separation.

Results

A Cylindrical Array of Cohesin in Mitosis

We have determined the three-dimensional (3D) distribution of cohesin in mitotic cells by using two core cohesin components, Smc3 and Mcd1/Scc1, and a SPB protein (Spc29) expressed from their endogenous promoters and fused to green or red fluorescent protein, respectively (GFP, RFP). In the sagittal section (side view of the mitotic spindle, Figure 2A, schematic), Smc3-GFP and Scc1-GFP are concentrated in two fluorescent lobes between the poles of the mitotic spindle (Smc3-GFP, Spc29-RFP, Figure 2A; Scc1-GFP, Spc29-CFP, Figure S1A available online). The peak intensity of fluorescence is 2.23 ± 0.43 times the intensity of cohesin in nuclear regions away from the spindle. In the transverse section (end-on view of the mitotic spindle, Figure 2B, schematic), Smc3-GFP forms an apparently hollow ring centered about the spindle axis (Smc3-GFP, Spc29-RFP, Figure 2B). There are numerous cohesin subunits concentrated in a cylindrical array around the mitotic spindle. To determine the height of the cylindrical array, we drew linescans through the long axis of fluorescence in Figure 2A. The distance between the half-maximum positions of the fluorescence intensity from one end of the cylinder to the other is 586 ± 105 nm (Figure 2A, n = 42, schematic in Figure 2G). The width of the cylindrical array was determined by taking 3D stacks of images through sagittal (Figure 2C) and transverse (Figure 2D) planes and measuring the distance between maximal fluorescence values of each peak (sagittal, Figures 2E and 2G; transverse, Figures 2F and 2H). The distance between the bilobed peaks of fluorescence is 293 ± 56 nm (sagittal plane, Figures 2E and 2G) versus 365 ± 51 nm (transverse plane, Figures 2F and 2H). The distance between the two peaks is constant through the entire height of the cylinder (3D stacks of transverse sections at 100 nm steps, Figure 2D). The decreased width measurement through the short axis of the bilobed fluorescence in the sagittal section (Figures 2A, 2C, and 2E) reflects variation that arises from off-centered sections. If the aperture of the cylindrical array was less than 350 nm in diameter, the objective point-spread function (Airy disk) would preclude the appearance of a hole in the cohesin fluorescence (Figure S1B). This pattern of cohesin fluorescence is indicative of a cylindrical array ~350 nm in width and ~600 nm in height.

To determine the relationship of the cylindrical array of cohesin with respect to kinetochore microtubules and the metaphase spindle, we examined strains containing Smc3-GFP and Ndc80-Cherry (Ndc80, an outer-kinetochore-complex member) (Figures 3A and 3B) or Tub1-CFP (Figures 3C and 3D). In the sagittal view, clusters of Ndc80-Cherry cap the fluorescent cohesin lobes (Figure 3A) and the valley of SMC3-GFP fluorescence coincides with the position of interpolar microtubules (Figure 3C). In the transverse view, Ndc80-Cherry is surrounded by a ring of Smc3-GFP (Figure 3B) and the spindle is centrally aligned (Figure 3D). Thus Smc3-GFP is distributed cylindrically around central spindle interpolar microtubules and spans ~75% of the distance between separated clusters of kinetochores in metaphase (~600 nm cohesin versus 800 nm kinetochore clusters).

Cohesin is associated with chromosomes from G_1, promoting cohesion upon replication and persisting until the onset of anaphase. In live cells, Smc3-GFP is seen to accumulate near the SPB in S phase (Figures S1D–S1F). However, the cylindrical array is only apparent after DNA replication and bipolar-spindle formation. To address the extent of DNA replication required for the cylindrical array, we examined Smc3-GFP in cells treated with hydroxyurea (HU) (Figure 3E). In the presence of HU, only early origins of replication are activated, and the bulk of chromosome replication is severely delayed or arrested [12]. Centromere-DNA replication is under the control of early-firing origins. Upon HU treatment, cells arrest with bipolar spindles and bioriented chromosomes, visualized by two centromere-proximal lacO spots, reflecting the replication of centromere DNA (Figure S2) [6]. The dimensions and intensity of Smc3-GFP are indistinguishable in HU-treated versus nontreated cells (Figure 3E). Replication of centromeric regions and subsequent biorientation is therefore sufficient for establishment of cohesin into a cylindrical array surrounding the central spindle.

Stability of Pericentric Cohesin

Upon anaphase onset, a subunit of cohesin (Scc1) is cleaved by separase [13], the spindle elongates (anaphase B), and sister kinetochores migrate to opposite poles (anaphase A). Anaphase

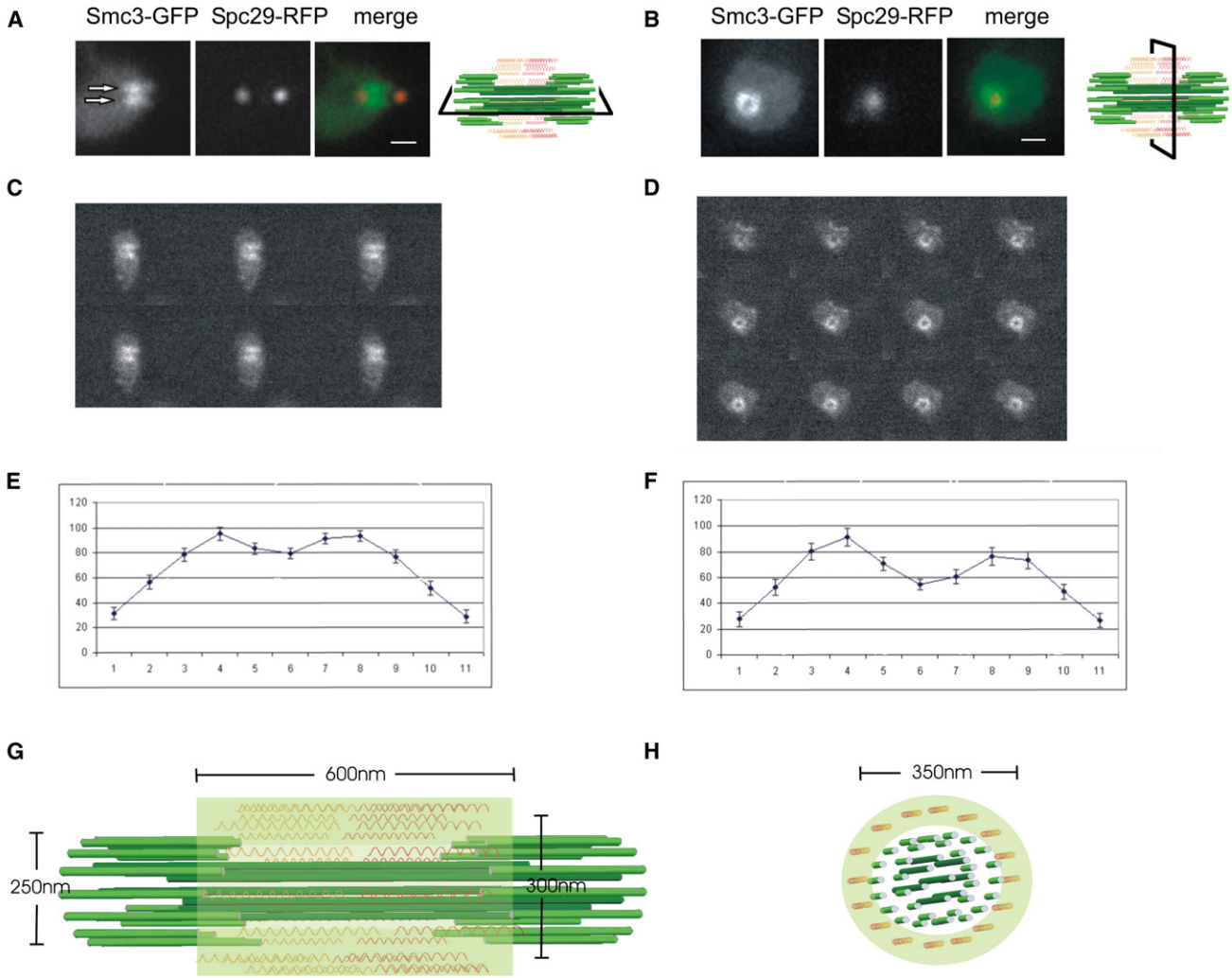

Figure 2. Distribution of Smc3-GFP in Metaphase

(A) Smc3-GFP is concentrated between the spindle-pole bodies in metaphase. Two oblongate lobes of fluorescence (arrows in Smc3-GFP image, green in overlay) with a dimmer area between are aligned between the spindle poles in a sagittal view of the spindle (Spc29-RFP, red in overlay). The schematic (right) illustrates the image plane of cohesin relative to the mitotic spindle in the sagittal view. Spindle length = 1.2 μm. Scale bar represents 1 μm.

(B) A cylindrical array of Smc3-GFP is visible in a transverse view of the spindle. Note the circular distribution Smc3-GFP (green in overlay) relative to the spindle-pole body (Spc29-RFP, red in overlay). The schematic (right) illustrates the image plane of cohesin in transverse view.

(C) Confocal serial sagittal sections of Smc3-GFP.

(D) Confocal serial transverse sections of Smc3-GFP. The bilobed fluorescence is qualitatively visible above background through ~600 nm (on average 6.4 ± 0.9 100 nm steps, n = 8) from the sagittal view and ~1000 nm (on average 7.8 ± 1.9 100 nm steps, n = 10) from the transverse view. A cylinder with a diameter of ~350 nm and height of ~600 nm would be seen through greater than 4 100 nm steps in the sagittal view, and greater than 7 100 nm steps in the transverse view when the decreased resolution due to the point-spread function (PSF) of the microscope objective in the z axis is taken into account. The number of steps in the sagittal and transverse views is consistent with the fluorescence measurements of the cylinder's height and diameter.

(E) Linescan through the oblongate lobes of Smc3-GFP fluorescence in the sagittal view. Error bars are standard error of the mean (SEM) (average of 53 cells).

(F) Linescan through Smc3-GFP fluorescence in the transverse view. Error bars are SEM (average of 22 cells). Arbitrary fluorescence units (y axis) are plotted versus distance in pixels (x axis, 65 nm/pixel).

(G) Model for pericentric cohesin in sagittal view. The mitotic spindle comprises 32 kinetochore MTs (16 in each half spindle, light green) and eight interpolar MTs (four from each pole, dark green), 250 nm in diameter. The distribution of cohesin is depicted as a transparent cylinder 600 nm in height and 300 nm in width. Pericentric DNA associated with cohesin is depicted as springs (orange) that span the distance between kinetochore microtubules.

(H) Model for pericentric cohesin in transverse view. Spindle microtubules (green) are surrounded by the cylindrical array of cohesin (transparent green). The position of pericentric DNA (orange) is based upon cohesin binding pericentric chromatin. The diameter of the cylindrical array in the transverse section is ~350 nm.

onset is defined as spindle elongation (13–14 min, Figure 4A). The fluorescence intensity of pericentric and arm cohesin was plotted as a function of time from metaphase to anaphase (Figure 4A, graph). Cohesin fluorescence decreased on average 66% between 2 and 6 min upon the onset of anaphase (n = 6). Pericentric cohesin is lost at or slightly before pole separation (Figure 4A, top). No overall change in Smc3 arm fluorescence is detected from metaphase to the end of anaphase.

The number of cohesin complexes holding the pericentric DNA structure together is crucial for understanding the

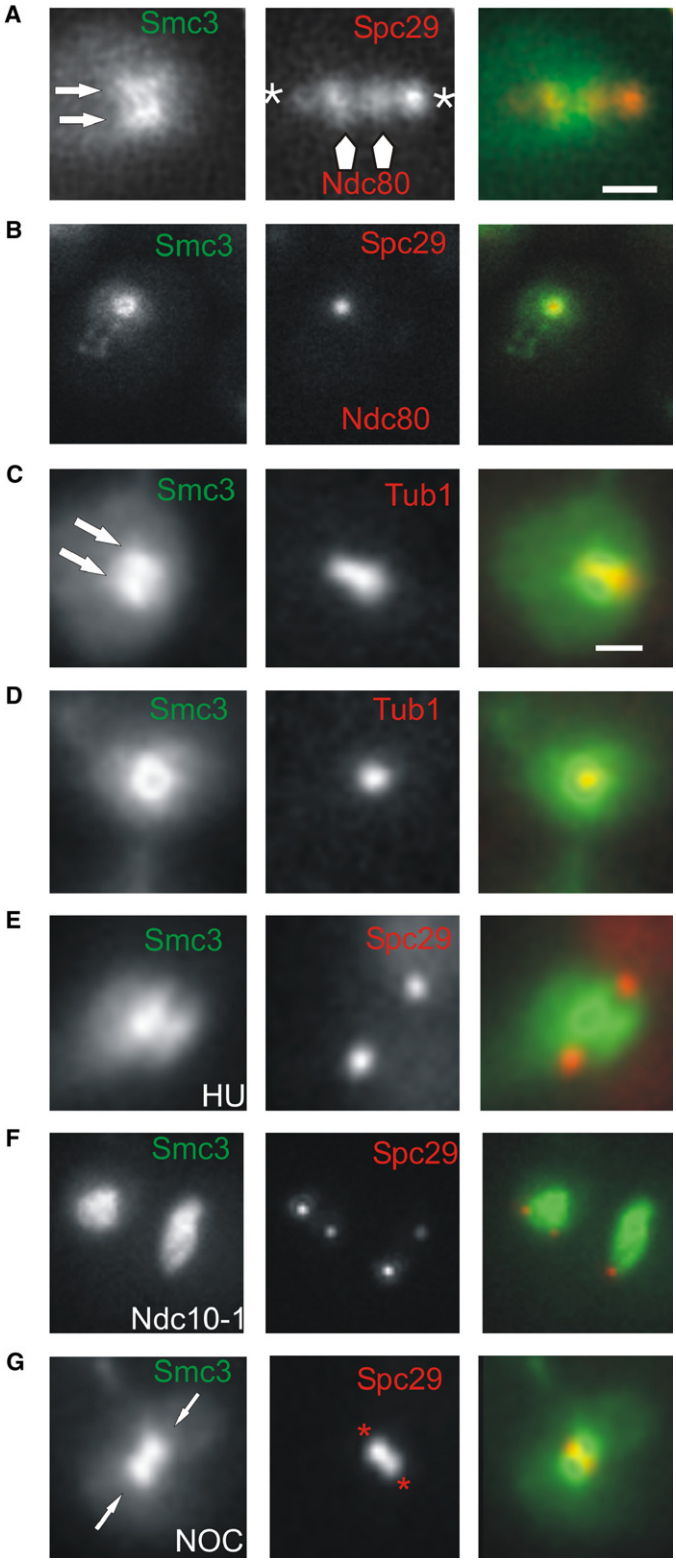

Figure 3. Position and Functional Requirements for the Cylindrical Array of Cohesin

(A) Colocalization of Smc3-GFP (left), Ndc80-Cherry (arrows), and Spc29-RFP (asterisks) (middle) in the sagittal section. The overlay (right) is a merge of both channels: Smc3-GFP, green; Spc29-RFP and Ndc80-Cherry, red.

(B) Colocalization of Smc3-GFP, Ndc80-Cherry, and Spc29-RFP in the transverse section. Smc3-GFP appears as a cylinder. Ndc80-Cherry resides within the cohesin cylindrical array.

(C) Colocalization of Smc3-GFP and Tub1-CFP in the sagittal section. The bilobed fluorescence of Smc3-GFP encircles Tub1-CFP (red in merge).

(D) Colocalization of Smc3-GFP and Tub1-CFP in the transverse section. The cylindrical array of Smc3-GFP encircles Tub1-CFP (red in merge).

(E) Smc3-GFP and Spc29-RFP localization after incubation with hydroxyurea (HU) for 3 hr. A bipolar spindle is formed (middle), and Smc3-GFP is concentrated in a bilobed structure (left) that lies between the two spindle poles. Smc3-GFP is shown in green and Spc29-RFP in red in the merge.

(F) Smc3-GFP distribution in the absence of functional kinetochores. Cells containing a temperature-sensitive allele of *ndc10-1* were grown at the restrictive temperature. There is no structural organization of Smc3-GFP. Smc3-GFP is shown green and Spc29-RFP in red in the merge.

(G) Smc3-GFP distribution after 2 hr incubation in 20 μg/ml nocodazole (NOC). The spindle has collapsed, as evidenced by the appearance of adjacent spindle pole bodies that mark the former spindle axis (middle, asterisks in red). Smc3-GFP remains concentrated proximal to the spindle poles in nocodazole-arrested cells (arrows in GFP panel and overlay). Two lobes of Smc3-GFP flank a dimmer area in which the collapsed spindle poles lie. Linescan through Smc3-GFP after spindle collapse is similar in shape to linescans of Smc3-GFP in untreated cells (see Figure S4). The fluorescence intensity of Smc3-GFP lobes in cells with collapsed spindles is 2–3× brighter than in untreated cells (see Figure S4). Smc3-GFP is shown in green and Spc29-RFP in red in the merge.

dynamic extension-relaxation behavior of pericentric chromatin observed during metaphase centromere movements. Using a comparative measurement of Smc3p-GFP fluorescence signal (to a known number of two Cse4 molecules per kinetochore [14]), we estimate that there are 108 ± 40 (n = 7) molecules in the pericentric region of cells containing Smc3-GFP (Table S1). The concentration of cohesin increases in the absence of tension to 222 ± 103 molecules/pericentric region (n = 11). These measurements translate to a minimum of 3.5 cohesin complexes per C loop (108 Smc3 molecules/32 centromeres). On the basis of centromere dynamics to deduce the amount of DNA in each C loop under tension in metaphase [9], we estimate that there is one cohesin complex every 4 kb, or one complex every 20 nucleosomes. The measurements are consistent with distribution of cohesin from chromatin-immunoprecipitation experiments [4, 15] and the ~2.5 fold increase in cohesin along pericentric chromatin in the absence of tension [16].

Considering that sister-kinetochore separation is dynamic, we have addressed whether cohesin within the pericentric chromatin is stably bound. Fluorescence recovery after photobleaching (FRAP) was used to quantitatively monitor cohesin stability in metaphase cells expressing Smc3-GFP (Figure 4B). In metaphase, one lobe of the GFP-cohesin cylinder was selectively targeted with a 200 ms laser exposure, whereas the other lobe retained fluorescence. Fluorescence of the bleached area was measured at 30 s intervals for 5 min. Comparison of integrated intensity measurements from the two sides of the cylinder revealed that cohesin fluorescence recovered above the background in only two of 20 cells analyzed. No significant fluorescence loss in the unbleached lobe was detected (data not shown). These results suggest that once assembled, cohesin is stably bound to pericentric chromatin. In contrast, FRAP of histone H2B-GFP (an exchangeable component of the nucleosome [17]), revealed

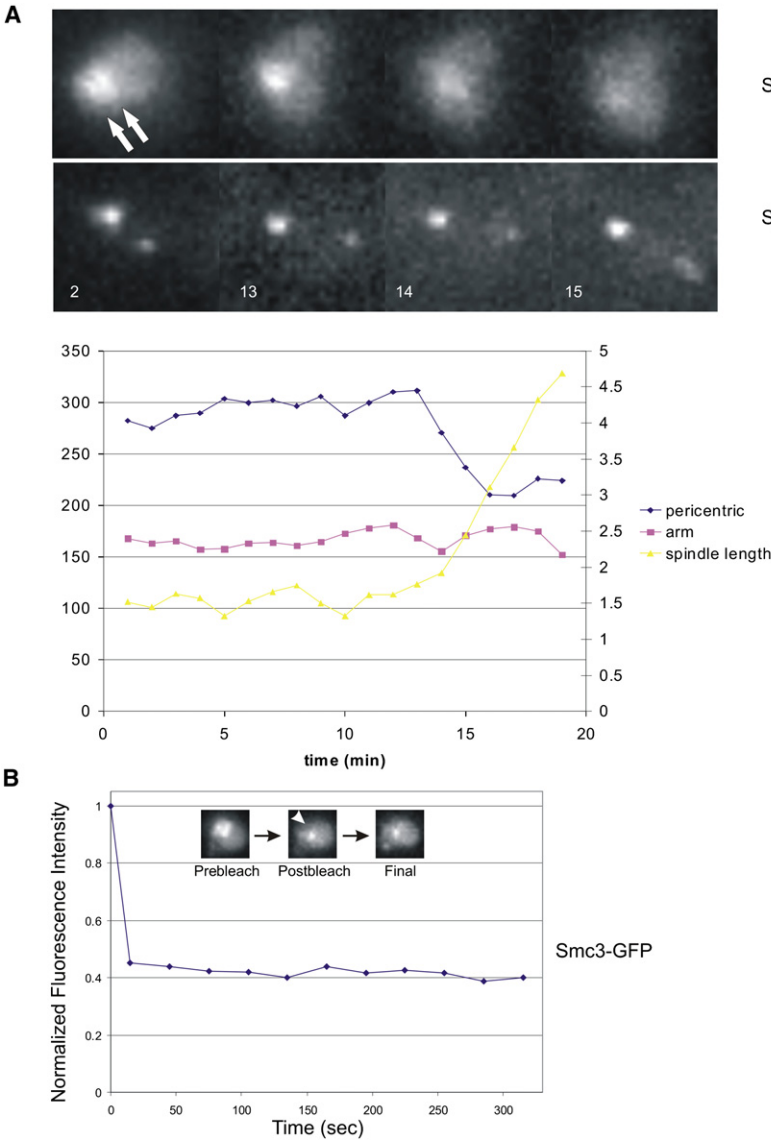

Figure 4. Cohesin Stability

(A) Loss of the cylindrical array in early anaphase. A time-lapse series of Smc3-GFP is shown as cells progress from metaphase to anaphase. The concentration of Smc3-GFP fluorescence is visible in metaphase between the spindle poles (2 min, top left, Smc3-GFP; bottom left, Spc29-RFP) (minutes indicated in bottom left corner). The fluorescence intensity between the two poles decreases between 13 and 14 min as the spindle elongates in anaphase (increase in distance between Spc29-RFP spindle poles, bottom panel). The difference in fluorescence intensity of spindle poles reflects the maturation time for RFP fluorescence in the new pole (to the right, bottom panel). Fluorescence intensity of Smc3-GFP was determined as described in the Experimental Procedures and plotted as a function of time in the bottom graph (left axis in arbitrary units, fluorescence intensity; right axis in microns, spindle length). Slightly before or concomitant with spindle elongation, the fluorescence intensity between the spindle poles decreases.

(B) Stability of cohesin in the cylindrical array. Fluorescence recovery after photobleaching (FRAP) was measured to determine cohesin stability in the pericentric region in cells expressing Smc3p-GFP. An argon laser attached to an inverted fluorescence microscope was directed to a portion of Smc3-GFP between the spindle poles (prebleach). GFP within a diffraction-limited spot (~0.25 μm) was bleached (postbleach). Images were acquired every 30 s for 5 min following photobleaching. As shown in the graph no recovery of Smc3-GFP fluorescence was detected. Cohesin fluorescence recovery above the background was apparent in only two of 17 cells.

that 37% ± 12% of H2B was dynamic in ten out of ten cells analyzed (exchanging with $t_{1/2}$ = 67 ± 16 s) (data not shown).

Chromosome Conformation at the Centromere

If the cylindrical distribution of cohesin reflects the geometric array of bioriented sister chromatids in mitosis, then separated sister kinetochores and flanking pericentric chromatin may be paired via intramolecular rather than intermolecular contacts [18]. To examine the conformation of pericentric DNA in vivo, we utilized an inverse-PCR strategy to map chromosome conformation (3C) [19]. Inverse primer pairs used to map the conformation of chromatin are shown in Figure 5A (pericentric chromatin P_1, P_2, and P_3; arm chromatin A, 75 kb from the centromere). Upstream and downstream primer pairs $P_{1u} + P_{1d}$ and $A_u + A_d$ are separated by the same physical distance (15 kb) in the genome. Chromatin was fixed by treatment of cells with formaldehyde, and the chromatin was digested with XbaI and ligated under dilute conditions to minimize intermolecular reactions. Each primer is ~200 bp downstream from an XbaI site resulting in PCR products of 400 bp when fragments containing sites complementary to the respective oligonucleotides ($P_{1u} + P_{1d}$ and $A_u + A_d$) ligate. For quantitation of random association due to thermal motion, ligation was also performed in the absence of crosslinking. Primer pairs from the chromosome arm ($A_u + A_d$) provide a control template to account for template yield in each experimental preparation.

In the absence of crosslinking, the ratio of PCR products from the pericentric versus arm chromatin (primer pairs P versus A) was 1.25 ± 0.15 (Figure S3B). This ratio could reflect greater ligation efficiency between fragments spanning the XbaI junction flanked by $P_{1u} + P_{1d}$ versus $A_u + A_d$, or it could reflect a more efficient PCR reaction with primer pairs $P_{1u} + P_{1d}$ versus $A_u + A_d$. To address the source of the difference and to ensure that the PCR reactions were linear over the range of input DNA, we constructed the template for inverse primer pairs $P_{1u} + P_{1d}$ and $A_u + A_d$. Templates were constructed by amplification of DNA from each primer to its respective XbaI site ($P_{1u} \rightarrow$ XbaI, $P_{1d} \rightarrow$ XbaI; and $A_u \rightarrow$ XbaI, $A_d \rightarrow$ XbaI, as shown in Figure 5A). The fragments were digested with XbaI and appropriate fragment pairs were ligated ($P_{1u} + P_{1d}$; $A_u + A_d$) and amplified with primer pairs $P_{1u} + P_{1d}$ or $A_u + A_d$. The yield of each product was quantitated by gel electrophoresis and absorbance at A_{260}. PCR was performed over a range of template DNA concentration (Figure S3A). At an input ratio of 1:1 P:A template, the mean ratio of PCR products was 1.21. This value was constant over a 10-fold range of input DNA concentration (Figure S3A). The ratio of the PCR products with primer pairs P versus A in the uncrosslinked sample (above) reflect equal

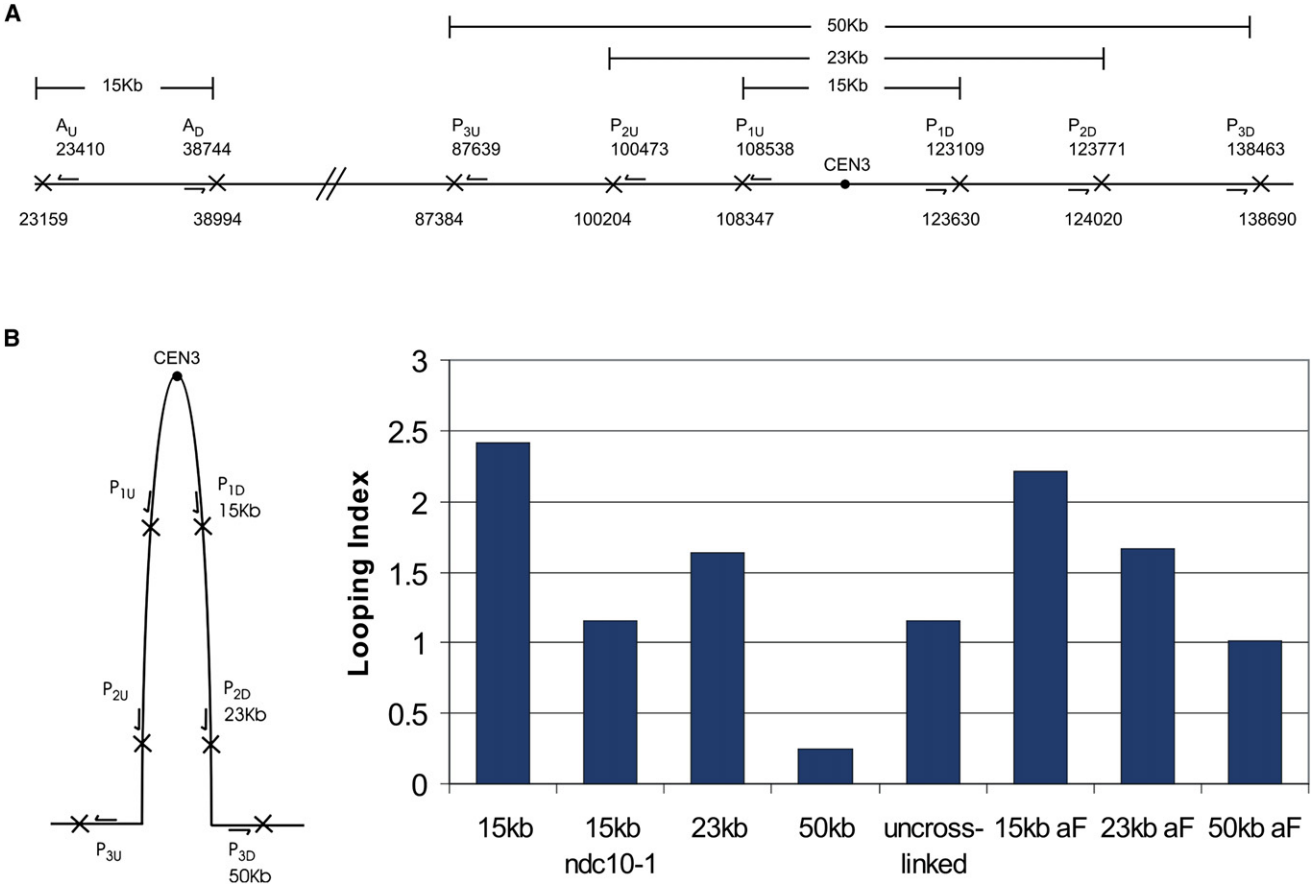

Figure 5. 3C Assay for Intramolecular Looping

(A) The schematic shows the position of oligonucleotide primers on chromosome III (arrows) relative to the centromere (filled circle). Each pair of oligonucleotides (P_{1u} + P_{1d} and A_u + A_d; *p*ericentric versus *a*rm chromatin) extend away from each other on the linear chromosome. XbaI sites are indicated by (X) downstream of each oligonucleotide primer. In the linear chromosomal configuration, these oligonucleotides will not prime DNA synthesis after the 3C assay. If there is intramolecular looping (as diagrammed in [B], left), the P_{1u} + P_{1d} oligonucleotides will prime DNA synthesis. The products from PCR reactions following crosslinking, restriction digestion, and ligation were quantified as described in the Experimental Procedures.

(B) Left: schematic representation of the extent of the intramolecular loop. Right: looping index for each experimental sample. The looping index accounts for differential efficiency of PCR reactions with primer set P versus A at an equivalent ratio of input template (see complete description in Figure S3). A looping index of 1 indicates equal concentration of input template for pericentric and arm products, respectively. Experimental samples (wild-type [WT], αF, *ndc10-1*, and uncrosslinked) were prepared as described in the Experimental Procedures.

concentration of the respective pericentric (P) or arm (A) templates after the sample preparation.

The experimental pericentric:arm (P:A) product ratios plotted against reconstructed P:A input ratios over the range of 0.3–5.0 are shown in Figure S3A. There is a linear relationship over a 10-fold range (6.6–66 picograms) of template DNA. All subsequent analysis was performed within the linear range of these 3C PCR reactions. The plot accounts for the different PCR efficiency of the primer sets and provides a standard for calibrating the degree of intramolecular looping from the experimental sample. We thus define a "looping index" as the ratio of P:A normalized for differences in PCR efficiency. A looping index of ~1.0 reflects an equal concentration of input pericentric and arm products, indicative of an equal propensity for arm or pericentric chromatin to loop (uncrosslinked sample, Figure 5B; P:A product ratio of 1.25, Figure S3B). For example, in the crosslinked samples amplified with the 15 kb primer pair (7.5 kb on either side of CEN3), there is a P:A product ratio of 1.96 (Figure S3B) and a looping index of 2.41 (Figure 5B). Thus pericentric chromatin DNA is 2.4× more prone to adopt an intramolecular loop (C loop) relative to arm DNA (Figure 5B). This increase in looping index (2.41) is comparable to the increased crosslinking efficiency reported by Dekker et al. [19] for the chromosome III centromere.

To determine the physical length of the intramolecular loop, we designed additional primer pairs spanning 23 kb (P_{2u} + P_{2d}) and 50 kb (P_{3u} + P_{3d}) of pericentric DNA (~11.5 and 25 kb on either side of CEN3, respectively) (Figures 5A and 5B). The pericentric:arm product ratio of uncrosslinked DNA varies with each primer pair (1.04 ± 0.03 and 2.16 ± 0.3 for the 23 kb and 50 kb primer pairs, respectively, see Figure S3B). After crosslinking, the Cen:arm product ratio increased by 24% (1.64 looping index) for the 23 kb primer pair and decreased 43% (0.25 looping index) for the 50 kb primer pair. The looping index for the 50 kb primer pair in the absence of DNA replication is 1.01 (αF 50 kb, Figure 5B). The 0.25 looping index obtained in logarithmic-phase growth indicates that the conformation of chromatin 25 kb on either side of the centromere is anticorrelated with intramolecular looping and may be constrained in its ability to adopt certain conformations. These results extend conclusions from examination of sister chromatids with lacO operators at various positions from the centromere [9] and indicate

Table 1. Looping Index for Wild-Type and Mutant Strains

Condition and Fragment Size	Looping Index
WT 15 kb	2.41
WT 23 kb	1.64
WT 50 kb	0.25
mcd1-1 15 kb	1.54
ndc10-1 15 kb	1.15
ndc10-1, αF 15 kb	1.15
αF 15 kb	2.31
αF 23 kb	1.67
αF 50 kb	1.01
galcen 15 kb	1.18
uncrosslinked	1.15

The looping index is a measure of the propensity for two regions of chromosome III to interact after crosslinking, restriction digestion, and ligation. The looping index is detailed in the text and Figure S3.

that intramolecular looping extends beyond 11.5 kb but not 25 kb on either side of the centromere.

The intramolecular pericentric loop is completely dependent upon kinetochore function. Ndc10 is one of the centromere-DNA binding factors (CBF3) and is essential for kinetochore formation [20]. The looping index for pericentric chromatin in *ndc10-1* mutant cells at the restrictive growth temperature is 1.15, equivalent to the uncrosslinked sample (Figure 5B and Figure S3). Because Ndc10 has been shown to bind additional sites in the genome [21], we utilized an alternative strategy to disrupt kinetochore function. Induction of a transcriptional promoter adjacent to the centromere results in loss of segregation function [22]. Cells containing a conditionally functional centromere (GALCEN3) were transferred to media containing galactose to activate the GAL1 promoter. The looping index of pericentric chromatin flanking an inactive centromere was 1.18 (Table 1 and Figure S3A). Ndc10 is depleted at the GALCEN locus [23], and therefore intramolecular looping of pericentric chromatin is dependent upon a functional kinetochore.

Upon loss of kinetochore function, there is concomitant loss of the cylindrical cohesin array. *ndc10-1* mutants at restrictive temperature no longer organize cohesin into a cylinder around the mitotic spindle (Figure 3F). Likewise, upon disruption of microtubule attachment in the Ndc80 outer kinetochore complex (*nuf2-45* mutants), Smc3-GFP is randomly distributed in the nucleus and visible as puncta of various sizes and positions relative to the spindle poles (Figure S1C).

To determine whether sister chromatids are required for C loop formation, we examined the structure of pericentric chromatin in cells arrested prior to DNA replication (via αF treatment). The looping index for the 15 kb primer pair (7.5 kb on either side of the centromere) was 2.31 in cells treated with αF (Table 1, Figure 5B, and Figure S3A), and the loop extends a physical distance comparable to that observed in logarithmic growing cells (Figure 5B, wild-type [WT] 23 kb 1.64, αF 23 kb 1.67). In contrast, the looping index for 50 kb of pericentric DNA (0.25) increased to 1.01 in αF-treated cells (Figure 5B and Figure S3B). Thus DNA sequences 25 kb on either side of CEN3 exhibit prior to DNA replication random associations comparable to those measured in uncrosslinked controls at 50 kb (Figure S3B). Upon replication, chromatin at the base of the C loop is held via cohesin-mediated sister-chromatid linkages, and the efficiency of ligation 25 kb on either side of CEN3 drops precipitously (Figure 5B).

An alternative strategy to address the role of sister chromatids is through the use of mutations in cohesin subunit Mcd1/Scc1. Mcd1 is expressed late in G1 and is largely absent from chromosomes prior to Start [24, 25]. *mcd1-1* mutants arrested with a metaphase-like spindle and prematurely separated sister chromatids. The looping index is 1.54 in *mcd1-1* mutants (Table 1 and Figure S3A). The reduction in looping index reflects a reduction in the number or length of intramolecular loops in the population or an increased distance between the two strands. Although cohesin is not required for loop formation, cohesin does contribute to the stability, extent, or proximity of the intramolecular loops.

Cohesin Contributes to Spindle-Length Control

The physical arrangement of pericentric chromatin in intramolecular loops predicts that chromatin may be a mechanical component of the spindle [8, 26–28]. Bouck and Bloom have shown that reduction of histone expression leads to increased spindle length in metaphase [26]. If cohesin contributes to the physical properties of pericentric chromatin, reduction of cohesin is likewise expected to influence metaphase spindle length. Spindle length was measured in *mcd1-1* mutants grown at permissive and restrictive conditions. *mcd1-1* mutants arrest primarily in mitosis, but the mutation does not prevent anaphase A (chromosome-to-pole movement) or exit from mitosis [29]. To examine spindle length in cells prior to anaphase onset, we introduced lacO arrays into the *LYS2* gene on chromosome II in *mcd1-1* mutants [30]. Only cells with separated sister chromatids in metaphase (separated lacO spots, but spots not at spindle poles) were examined. Metaphase spindle length was 1.44 ± 0.32 (n = 61) at 25°C. Spindle length increased to 2.35 ± 0.77 (n = 27) upon shift to 37°C. This is comparable to the increase in spindle length upon reduction of histone H3 (from 1.47 ± 0.28 n = 71 to 2.33 ± 0.40, n = 77 [26]). A corollary to the hypothesis for pericentric chromatin as an extensible element of the spindle is that upon spindle collapse the chromatin should relax and the cylindrical distribution should be compacted. For examination of the distribution of Smc3-GFP in the absence of tension, cells were treated with nocodazole to depolymerize microtubules and collapse the spindle (Figure 3G). The concentration of cohesin increases in the vicinity of the spindle poles after spindle collapse (Figure 3G and Figure S4). These data are indicative of the inward recoil of the pericentric chromatin relative to spindle poles upon spindle collapse and are consistent with the finding that cohesin accumulates within pericentric chromatin in the absence of tension [16].

Discussion

The simple budding-yeast spindle with its complete genomic sequence including the centromeres is an excellent model from which to deduce the contribution of microtubules and chromosome organization to spindle function. Sixteen kinetochore microtubules on average 0.35 μm in length and four interpolar microtubules ~1 μm in length emanate from each spindle pole. Kinetochores from each of the 16 chromosomes cluster into a diffraction-limited spot, and upon biorientation appear as two clusters in mitosis. We provide evidence for the structural basis for kinetochore biorientation. Pericentric cohesins are organized in a cylindrical array around the metaphase spindle. Each sister chromatid adopts an intramolecular loop (C loop) with centromere DNA proximal to the kinetochore MT plus-end at the apex of the loop that spans a region of 25 kb flanking the 125 bp centromere core (Figure 6A). Pericentric chromatin spans the distance between clusters of 16 bioriented kinetochores, resulting in a cylindrical array of the 32

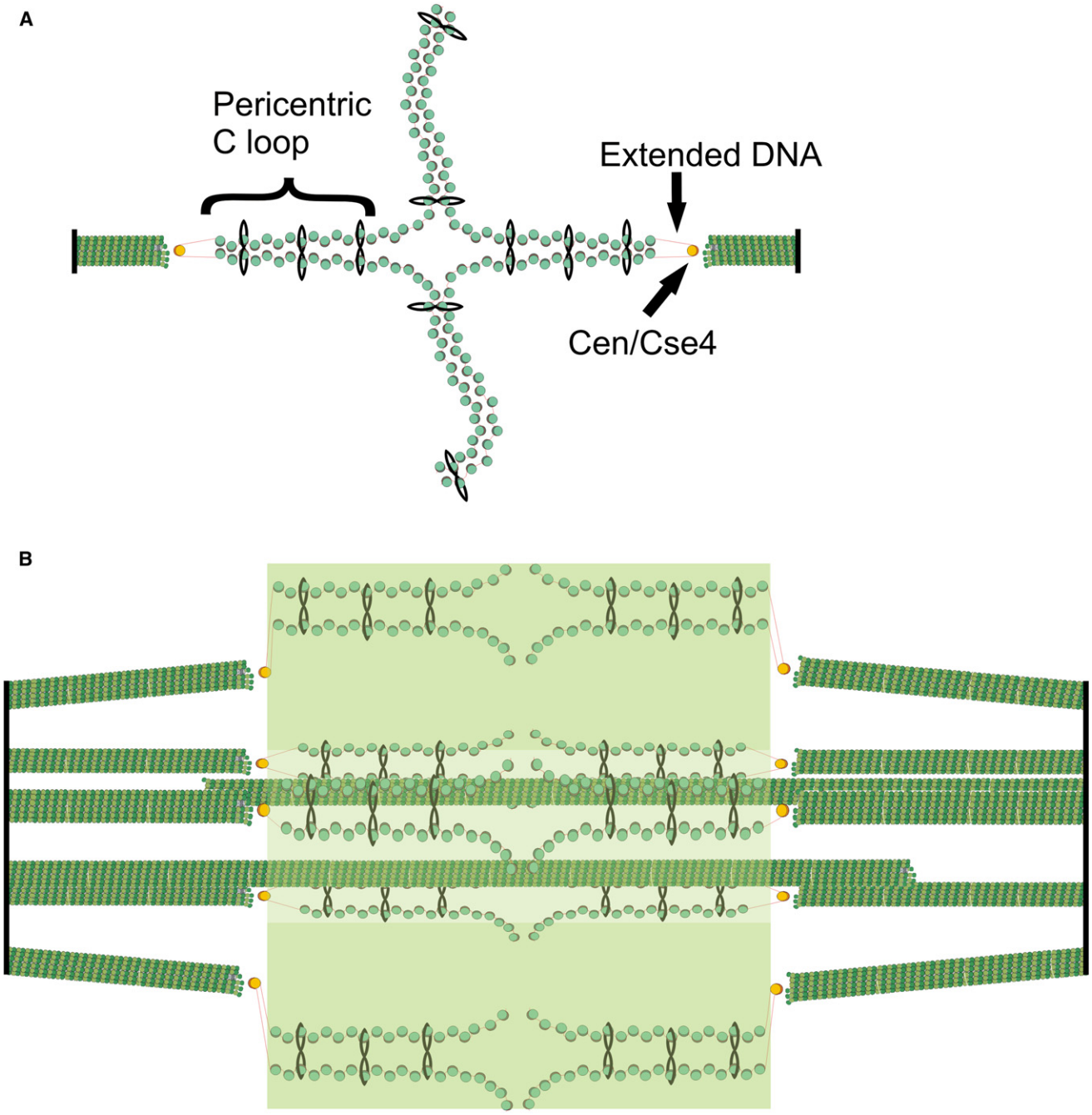

Figure 6. Model of the Organization of Cohesin and Pericentric Chromatin in Metaphase

(A) DNA of each sister chromatid is held together via intramolecular bridges that extend approximately 11.5 kb on either side of the centromere. A transition from intra- to intermolecular linkages results in a cruciform structure.

(B) Five (of 16) bioriented sister chromatids are shown with two (of eight) interpolar microtubules. We have proposed that the transition between intramolecular looping and intermolecular cohesion is mobile and on average 7 kb from the centromere core [18]. DNA adjacent to the centromere may extend to its B form length in vivo (as described in text, depicted as red lines), thereby linking the centromere at kinetochore-microtubule plus ends to strands of intramolecularly paired pericentric chromatin and cohesin that are displaced radially from spindle microtubules. Microtubules and spindle-pole bodies are represented by green and black rods, respectively. The 125 bp centromere is wrapped around the Cse4-containing histone in yellow. Nucleosomal chromatin is depicted as green histone cores wrapped around DNA in red. Cohesin is depicted as black circles. The fluorescence distribution of cohesin is depicted in transparent green. Pericentric chromatin from each of the 16 chromosomes is displaced 70–90 nm radially from the central spindle microtubules. The entire spindle is composed of 32 kinetochore microtubules and eight pole-pole microtubules.

pericentric regions within the mitotic spindle (Figure 6B). This results in a cruciform configuration between sites of microtubule attachment and sister-chromatid pairing (Figure 6A). These loops of pericentric DNA together with cohesin may provide the mechanical linkage between separated sister kinetochores.

The discovery of intramolecular looping at the centromere provides a solution to the major paradox in understanding

the accumulation of cohesin at sites of separated sister DNA strands. Cohesin is organized into a supramolecular cylindrical array encompassing the mitotic spindle. From the fluorescence distribution and the spread of light through the objective (point-spread function), we estimate the dimensions of the cylindrical array to be approximately 350 nm in diameter by 600 nm in length. The diameter of the cohesin cylinder is approximately 70–80 nm larger than measured for the diameter of the spindle microtubules in yeast by electron microscopy [31] and 200 nm shorter than the distance between clusters of microtubule plus ends (~800 nm) [32]. This difference in diameter is the basis for depicting cohesin and the pericentric C loops radially displaced from the spindle microtubules (Figure 6B). A question raised by these findings is how the pericentric chromatin is physically linked to the microtubule plus end. The centromeric nucleosome cluster, as visualized by Cse4 fluorescence, shows no such cylindrical array, and the cluster is very close to the microtubule plus end [33]. We can reconcile these findings by proposing that the plus ends of the kinetochore microtubules are very close to the Cse4 nucleosome, and the adjacent 70–90 bp of DNA flanking the Cse4 nucleosome spans the distance to the flanking chromatin (Figure 6B). Several features of the DNA flanking the 125 bp centromere are consistent with the idea that this DNA is in a B form configuration and devoid of protein. First, the concentration of cohesin is reduced at the centromere core and does not increase until 50–100 bp away from the centromere [15]. Second, nuclease-hypersensitive sites (70–90 bp) have been mapped to the region immediately flanking the 125 bp CEN [34]. Third, the region of pericentric chromatin is hyperstretched relative to chromosome arms in mitosis [9]. These data suggest that the 70–90 bp of DNA adjacent to the centromere may extend to its B form length in vivo (24–30 nm long), linking the centromere at kinetochore microtubule plus ends to strands of intramolecularly paired pericentric chromatin that are displaced radially from spindle microtubules (Figure 6B).

Cohesin deposition is dependent upon kinetochore function [3]. However cohesin is not essential for intramolecular looping (*mcd1-1*, Table 1), nor is tension (αF, Figure 5B and Table 1). In contrast, the loss of the inner centromere binding complex *ndc10-1* results in loss of the intramolecular loop. Ndc10, along with the other proteins that constitute the core centromere-DNA binding factor (CBF3), bends centromere DNA approximately 60° [35]. This deflection in DNA curvature may favor intramolecular loop formation. Cohesin contributes to the stability and/or extent of pericentric loop formation as evidenced by the fractional decrease in looping index (2.41 to 1.54 in *mcd1-1*). Cohesin remains concentrated in the vicinity of the spindle poles after spindle collapse with nocodazole (Figure 3G, Figure S4). The fluorescence intensity per pixel is 2–3 times brighter after spindle collapse (Figure S4), indicating that rather than pericentric chromatin unraveling into the nucleus, the chromatin is further condensed or compressed. If pericentric chromatin were inelastic, DNA strands would not be expected to remain aligned tightly with the two collapsed spindle poles. Alternatively, if pericentric chromatin were elastic, then upon loss of tension generated by microtubules, the chromatin would condense and retract adjacent to the collapsed spindle poles. The latter is observed experimentally and supports the view that this region behaves as spring-like element that generates an inward force [26–28].

Although individual strands of DNA may be quite weak springs, the spring constant of parallel arrays of springs is the sum of the individual spring constants. In addition, the intramolecular pairing of pericentric chromatin confers unique structural properties that may be important during mitosis. A two-fold increase in the radius of a filament increases its resistance to bending 16-fold. The additional loading of cohesin is very likely to reinforce the tensile strength of these loops, as demonstrated for the role of condensin in organizing rigid elastic chromosomes axes [36].

The depiction of the 16 microtubule attachment sites clustered around the mitotic spindle (Figure 6B) may be relevant to understanding the organization of regional kinetochores. Centromeres in budding yeast are small (125 bp) compared to those in other fungi (30–40 kb in *S. pombe*) and mammalian cells (~5 Mb). In contrast, the number of microtubules per chromosome is 1 in budding yeast, 2–3 in fission yeast, and 25–30 in mammalian cells. Why such a large disparity in centromere DNA content, and not in microtubule number? This range of DNA sequences specifying kinetochore formation has led to the classification of point versus regional centromeres [37]. If one considers that the centromere comprises the site for kinetochore-protein binding as well as pericentric flanking DNA, the ratio of pericentric DNA to microtubule may indeed scale throughout phylogeny (20 kb of pericentric chromatin per microtubule attachment site in yeast versus 1 Mb of centromeric chromatin per 30 microtubule attachment sites in mammalian cells = ~30 kb per attachment site). Furthermore, sister-centromere pairs are separated by similar distances when under tension (~2 μm, newt lung cell [38], versus ~0.8 μm, budding yeast [9]) despite extreme disparity in spindle size. The view of a cylindrical arrangement of pericentric chromatin and clustered kinetochores in yeast may reflect the structural basis for kinetochore function that is conserved throughout phylogeny. The basic subunit organization of the eukaryotic kinetochore is the single attachment site. However, multiple attachment sites can be clustered whether they are on separate chromosomes (as in yeast) or within a single chromosome (as in mammals). There is evolutionary and experimental precedence for the idea that kinetochores are clusters of individual attachment sites. Indian muntjac kinetochores (2n = 6) are thought to represent a centromere fusion evolved from the smaller Chinese muntjac progenitor (2n = 46) [39]. On the experimental side, Zinkowski et al. [40] were able to fragment kinetochores by inducing mitosis with unreplicated genomes. This led to the idea that the mammalian kinetochore is based on a repeat-subunit structure. The single microtubule binding site in budding yeast may be the conserved repeat subunit, and the cluster of 16 yeast kinetochores may be comparable to one mammalian kinetochore consisting of multiple attachment sites.

In summary, the cylindrical array of two cohesin subunits, Smc3 and Scc1, observed in vivo and the state of pericentric DNA as mapped by chromatin conformation indicate that pericentric chromatin is organized into an intramolecular loop that forms the basis of bioriented sister chromatids. The C loop structure reveals the geometrical basis for kinetochore biorientation and resolves the paradox of maximal interstrand separation in regions of highest cohesin concentration. The data indicate that the chromosome segregation apparatus is a composite structure of two biopolymers, centromere DNA loops and microtubules. C loops provide the compliant linkage between stiffer kinetochore microtubules. Cohesin contributes to the stability of the C loops, whereas the kinetochore provides the mechanical linkage between C loop DNA and microtubules. This intramolecular loop provides a physical mechanism for biorientation of sister kinetochores. Chromatin buffers mitotic forces on the chromosome throughout cycles

of microtubule growth and shortening. The chromatin loops described herein are reminiscent of DNA loops in mammalian kinetochores and may define the fundamental unit for microtubule attachment [40].

Supplemental Data

Additional Experimental Procedures, four figures, and one table are available at http://www.current-biology.com/cgi/content/full/18/2/81/DC1/.

Acknowledgments

This work was supported by a grant from the National Institutes of Health GM-32238 to K.S.B. We thank members of the laboratory for critical reading of the manuscript.

Received: November 1, 2007
Revised: November 28, 2007
Accepted: December 7, 2007
Published online: January 17, 2008

References

1. Huang, C.E., Milutinovich, M., and Koshland, D. (2005). Rings, bracelet or snaps: Fashionable alternatives for Smc complexes. Philos. Trans. R. Soc. Lond. B Biol. Sci. *360*, 537–542.
2. Nasmyth, K., and Haering, C.H. (2005). The structure and function of SMC and kleisin complexes. Annu. Rev. Biochem. *74*, 595–648.
3. Weber, S.A., Gerton, J.L., Polancic, J.E., DeRisi, J.L., Koshland, D., and Megee, P.C. (2004). The kinetochore is an enhancer of pericentric cohesin binding. PLoS Biol. *2*, E260.
4. Blat, Y., and Kleckner, N. (1999). Cohesins bind to preferential sites along yeast chromosome III, with differential regulation along arms versus the centric region. Cell *98*, 249–259.
5. Straight, A.F., Marshall, W.F., Sedat, J.W., and Murray, A.W. (1997). Mitosis in living budding yeast: Anaphase A but no metaphase plate. Science *277*, 574–578.
6. Goshima, G., and Yanagida, M. (2000). Establishing biorientation occurs with precocious separation of the sister kinetochores, but not the arms, in the early spindle of budding yeast. Cell *100*, 619–633.
7. He, X., Asthana, S., and Sorger, P.K. (2000). Transient sister chromatid separation and elastic deformation of chromosomes during mitosis in budding yeast. Cell *101*, 763–775.
8. Tanaka, T., Fuchs, J., Loidl, J., and Nasmyth, K. (2000). Cohesin ensures bipolar attachment of microtubules to sister centromeres and resists their precocious separation. Nat. Cell Biol. *2*, 492–499.
9. Pearson, C.G., Maddox, P.S., Salmon, E.D., and Bloom, K. (2001). Budding yeast chromosome structure and dynamics during mitosis. J. Cell Biol. *152*, 1255–1266.
10. Chen, Y., Baker, R.E., Keith, K.C., Harris, K., Stoler, S., and Fitzgerald-Hayes, M. (2000). The N terminus of the centromere H3-like protein Cse4p performs an essential function distinct from that of the histone fold domain. Mol. Cell. Biol. *20*, 7037–7048.
11. Pearson, C.G., Yeh, E., Gardner, M., Odde, D., Salmon, E.D., and Bloom, K. (2004). Stable kinetochore-microtubule attachment constrains centromere positioning in metaphase. Curr. Biol. *14*, 1962–1967.
12. McCarroll, R.M., and Fangman, W.L. (1988). Time of replication of yeast centromeres and telomeres. Cell *54*, 505–513.
13. Uhlmann, F., Lottspeich, F., and Nasmyth, K. (1999). Sister-chromatid separation at anaphase onset is promoted by cleavage of the cohesin subunit Scc1. Nature *400*, 37–42.
14. Joglekar, A.P., Bouck, D.C., Molk, J.N., Bloom, K.S., and Salmon, E.D. (2006). Molecular architecture of a kinetochore-microtubule attachment site. Nat. Cell Biol. *8*, 581–585.
15. Glynn, E.F., Megee, P.C., Yu, H.G., Mistrot, C., Unal, E., Koshland, D.E., DeRisi, J.L., and Gerton, J.L. (2004). Genome-wide mapping of the cohesin complex in the yeast Saccharomyces cerevisiae. PLoS Biol. *2*, E259.
16. Eckert, C.A., Gravdahl, D.J., and Megee, P.C. (2007). The enhancement of pericentromeric cohesin association by conserved kinetochore components promotes high-fidelity chromosome segregation and is sensitive to microtubule-based tension. Genes Dev. *21*, 278–291.
17. Jamai, A., Imoberdorf, R.M., and Strubin, M. (2007). Continuous histone H2B and transcription-dependent histone H3 exchange in yeast cells outside of replication. Mol. Cell *25*, 345–355.
18. Bloom, K., Sharma, S., and Dokholyan, N.V. (2006). The path of DNA in the kinetochore. Curr. Biol. *16*, R276–R278.
19. Dekker, J., Rippe, K., Dekker, M., and Kleckner, N. (2002). Capturing chromosome conformation. Science *295*, 1306–1311.
20. Goh, P.Y., and Kilmartin, J.V. (1993). NDC10: A gene involved in chromosome segregation in Saccharomyces cerevisiae. J. Cell Biol. *121*, 503–512.
21. Espelin, C.W., Simons, K.T., Harrison, S.C., and Sorger, P.K. (2003). Binding of the essential Saccharomyces cerevisiae kinetochore protein Ndc10p to CDEII. Mol. Biol. Cell *14*, 4557–4568.
22. Hill, A., and Bloom, K. (1987). Genetic manipulation of centromere function. Mol. Cell. Biol. *7*, 2397–2405.
23. Collins, K.A., Castillo, A.R., Tatsutani, S.Y., and Biggins, S. (2005). De novo kinetochore assembly requires the centromeric histone H3 variant. Mol. Biol. Cell *16*, 5649–5660.
24. Ciosk, R., Shirayama, M., Shevchenko, A., Tanaka, T., Toth, A., Shevchenko, A., and Nasmyth, K. (2000). Cohesin's binding to chromosomes depends on a separate complex consisting of Scc2 and Scc4 proteins. Mol. Cell *5*, 243–254.
25. Laloraya, S., Guacci, V., and Koshland, D. (2000). Chromosomal addresses of the cohesin component Mcd1p. J. Cell Biol. *151*, 1047–1056.
26. Bouck, D.C., and Bloom, K. (2007). Pericentric chromatin is an elastic component of the mitotic spindle. Curr. Biol. *17*, 741–748.
27. Nicklas, R.B. (1963). A quantitative study of chromosomal elasticity and its influence on chromosome movement. Chromosoma *14*, 276–295.
28. Nicklas, R.B. (1988). The forces that move chromosomes in mitosis. Annu. Rev. Biophys. Biophys. Chem. *17*, 431–449.
29. Guacci, V., Koshland, D., and Strunnikov, A. (1997). A direct link between sister chromatid cohesion and chromosome condensation revealed through the analysis of MCD1 in S. cerevisiae. Cell *91*, 47–57.
30. Lobachev, K., Vitriol, E., Stemple, J., Resnick, M.A., and Bloom, K. (2004). Chromosome fragmentation after induction of a double-strand break is an active process prevented by the RMX repair complex. Curr. Biol. *14*, 2107–2112.
31. Winey, M., Mamay, C.L., O'Toole, E.T., Mastronarde, D.N., Giddings, T.H., Jr., McDonald, K.L., and McIntosh, J.R. (1995). Three-dimensional ultrastructural analysis of the Saccharomyces cerevisiae mitotic spindle. J. Cell Biol. *129*, 1601–1615.
32. Gardner, M.K., Pearson, C.G., Sprague, B.L., Zarzar, T.R., Bloom, K., Salmon, E.D., and Odde, D.J. (2005). Tension-dependent regulation of microtubule dynamics at kinetochores can explain metaphase congression in yeast. Mol. Biol. Cell *16*, 3764–3775.
33. Pearson, C.G., Gardner, M.K., Paliulis, L.V., Salmon, E.D., Odde, D.J., and Bloom, K. (2006). Measuring nanometer scale gradients in spindle microtubule dynamics using model convolution microscopy. Mol. Biol. Cell *17*, 4069–4079.
34. Bloom, K.S., and Carbon, J. (1982). Yeast centromere DNA is in a unique and highly ordered structure in chromosomes and small circular minichromosomes. Cell *29*, 305–317.
35. Pietrasanta, L.I., Thrower, D., Hsieh, W., Rao, S., Stemmann, O., Lechner, J., Carbon, J., and Hansma, H. (1999). Probing the Saccharomyces cerevisiae centromeric DNA (CEN DNA)-binding factor 3 (CBF3) kinetochore complex by using atomic force microscopy. Proc. Natl. Acad. Sci. USA *96*, 3757–3762.
36. Almagro, S., Riveline, D., Hirano, T., Houchmandzadeh, B., and Dimitrov, S. (2004). The mitotic chromosome is an assembly of rigid elastic axes organized by structural maintenance of chromosomes (SMC) proteins and surrounded by a soft chromatin envelope. J. Biol. Chem. *279*, 5118–5126.
37. Pluta, A.F., Mackay, A.M., Ainsztein, A.M., Goldberg, I.G., and Earnshaw, W.C. (1995). The centromere: Hub of chromosomal activities. Science *270*, 1591–1594.
38. Waters, J.C., Skibbens, R.V., and Salmon, E.D. (1996). Oscillating mitotic newt lung cell kinetochores are, on average, under tension and rarely push. J. Cell Sci. *109*, 2823–2831.
39. He, D., and Brinkley, B.R. (1996). Structure and dynamic organization of centromeres/prekinetochores in the nucleus of mammalian cells. J. Cell Sci. *109*, 2693–2704.
40. Zinkowski, R.P., Meyne, J., and Brinkley, B.R. (1991). The centromere-kinetochore complex: A repeat subunit model. J. Cell Biol. *113*, 1091–1110.